ORIGINAL PAPER

CrossMark

A molecularly imprinted chitosan doped with carbon quantum dots for fluorometric determination of perfluorooctane sulfonate

Zhe Jiao[1,2] · Jingwen Li[1] · Liangji Mo[1] · Jinming Liang[1] · Hongbo Fan[1,2]

Abstract

A molecularly imprinted polymer (MIP) was fabricated for selective recognition of the highly persistent pollutant perfluorooctane sulfonate (PFOS). The MIP was prepared from chitosan and doped with fluorescent carbon quantum dots (CQDs). It was characterized by fluorescence spectrophotometry, scanning electron microscopy, and Fourier transform infrared spectroscopy. The fluorescence of the CQDs, best measured at excitation/emission wavelengths of 350/460 nm, is enhanced by PFOS, and the effect is much stronger for the MIP than for the nonimprinted polymer (NIP). The imprinting factor is 2.75. The method has good specificity over sodium dodecyl sulfate (SDS), perfluorooctanoic acid (PFOA), sodium dodecyl sulfonate (SDS'), sodium dodecyl benzene sulfonate (SDBS), perfluorooctanesulfonyl fluoride (POSF), perfluorobutane sulfonate (PFBS) and 1-octanesulfonic acid sodium (OSA). Fluorescence increases linearly in the 20–200 pg·L^{-1} POSF concentration range in aqueous solution. The method was applied to the determination of PFOS in spiked serum and urine samples. The limits of detection are 66 and 85 pg·L^{-1} for serum and urine samples respectively. The recoveries ranged from to 81–98%, with relative standard deviations in the range of 1.8–8.2%. Compared with LC-MS/MS, this assay is more convenient since the material can be prepared flexibly and the method can be applied on-site.

Keywords Molecular imprinting · Chitosan hydrogel · PFOS · Selective recognition · Fluorescence enhancement · Carbon quantum dots · Serum and urine samples

Introduction

Perfluorooctane sulfonate (PFOS) has been manufactured worldwide since the 1950s and is used as a raw material for the manufacture of textiles, cosmetics, and firefighting foams [1–3]. Due to the extremely strong carbon-fluorine bonds and its difficulty to degrade, it is considered to be persistent pollutant in environment. The PFOS has been found in serum samples due to human exposure to PFOS [4]. The current major analytical technique for PFOS determination is high-performance liquid chromatography (HPLC)-mass spectrometry (HPLC-MS) [5, 6]. Despite its good sensitivity, this protocol requires expensive, complex instrumentation, and complicated sample pretreatment. In addition to HPLC, photoelectrochemical [7], electrochemiluminescence [8], electrochemical [9], and fluorescent quantification [10] have also been applied for determination of PFOS.

Molecular imprinting is a technique to make a selective binding site for a specific chemical. The stability, ease of preparation, and low cost make the molecularly imprinted materials particularly attractive [11, 12]. Molecularly imprinted polymers (MIPs) have aroused extensive attention and been widely applied in many fields, such as solid-phase extraction, chemical sensing methods and artificial antibodies. Combining the high selectivity of MIPs and excellent optical properties of fluorescent nanoparticles would develop sensitive and specific methods for recognizing an analyte [13–17]. The MIPs on the surface can specially bind the target analyte, which bring about the fluorescence change, and the degree of change may be related to the amount of the target analyte. The combination of MIP with semiconductor quantum dots has been applied for selective determination of tetrabromobisphenol A [18],

pentachlorophenol [19], pyrethroids [20], 2,4,6-trinitrotoluene [21], etc. Apart from semiconductor QDs, graphene quantum dots [22], composition material of graphene oxide [23], and carbon quantum dots [24] were also incorporated to the MIP material as selective fluorescent sensor.

Carbon quantum dots (CQDs) have been attracting enormous attention due to their unique optical properties, good biocompatibility, hydrophilicity and nontoxicity [25]. Compared with the conventional semiconductor QDs, CQDs can be prepared by a simple, cost-effective and environmentally friendly approach. Huang el at reported one-step synthesis of fluorescent carbon dots with hydrothermal reaction [26], Zhang et al. reported a low-temperature solid-phase method to synthesize highly fluorescent carbon nitride dots with tunable emission [27]. CQDs has been reported for detection of phosphate in complicated matrixes [28], single particle dynamic imaging and Fe^{3+} sensing [29], as well as detection of mercury in environmental samples [30]. However, fluorescent detection based on CQDs often confronts with the interference of the coexisting substances. A feasible method to enhance the selectivity of fluorescent detection is the use of molecular imprinting technology. Chitosan is a cheap natural polymer and was used as MIP adsorbent to selectively remove PFOS from aqueous solution [31, 32]. Therefore, incorporation of CQDs into the chitosan-based MIP can be used for simultaneous sensing and removal of PFOS.

In this paper, we describe a highly selective molecularly imprinted fluorescent hydrogel for PFOS detection (Scheme 1). The CQDs were used as signal transducer and doped on the chitosan hydrogel through covalent bond during the polymerization reaction of chitosan with epichlorohydrin (ECH). The sulfonate group in the template molecule PFOS can interact with the amino groups (-NH$_2$) in the molecule of chitosan and CQDs to form a complex through hydrogen bonding or electrostatic interaction. After elution of the PFOS, many specific imprinted cavities with complementarity to PFOS were produced, and can generate a specific response to PFOS. The enhancement of PL intensity was observed in the presence of different concentrations of PFOS. The imprinting factor (IF) of the molecular hydrogel was evaluated for selectivity. The hydrogel was applied for PFOS detection in serum and urine samples, and the results were compared with LC-MS/MS.

Experimental

Reagents and instrumentation

Perfluorooctane sulfonate (PFOS, 98%), perfluorooctanoic acid (PFOA, 96%), perfluorobutane sulfonate (PFBS, 98%), and perfluorooctanesulfonyl fluoride (POSF, 95%) were bought from Shanghai Makclin Biochemical Co., Ltd.

(Shanghai, China, http://www.macklin.cn). Sodium dodecyl sulfate (SDS), sodium dodecyl sulfonate (SDS'), sodium dodecyl benzene sulfonate (SDBS), and 1-octanesulfonic acid sodium (OSA) were purchased from Aladdin Biochemical Co., Ltd.(Shanghai, China, http://www.aladdin-e.com). Citric acid, ethylenediamine, epichlorohydrin acetone (ECH), acetic acid and sodium hydroxide were purchased from Tianjin Damao Chemical Reagent Factory (Tianjin, China, http://www.aladdin-e.com). The regents were all analytical regents unless otherwise listed.

The photoluminescence (PL) spectra were recorded on Thermo Fisher Fluorospectrophotometer Lumina (Massachusetts, U.S., http://www.thermofisher.com), the measurements were performed with excitation wavelength at 350 nm, and emission wavelength at 460 nm. Agilent 1200 SL high performance liquid chromatograph (HPLC) interfaced with an Agilent 6400 Triple Quadrupole mass spectrometer (MS/MS) was used for monitoring the elution of template PFOS (California, U.S., https://www.agilent.com/). The UV and IR absorption spectra were recorded on Gensys 10S UV-VIS spectrophotometer and TJ270-30A Infrared spectrophotometer (Massachusetts, U.S., http://www.thermofisher.com). The TEM images were obtained by FEI Tecnai G200 high resolution transmission electron microscopy (http://www.fei.com, Oregon, USA). The SEM images were obtained by Zeiss Sigma 500 scan electron microscopy (Oberkochen, Germany, https://www.zeiss.com). X-ray diffractometer (XRD)spectrum were obtained by Rigaku UItima IV (Tokyo, Japan, http://www.rigaku.com), pH value was determined on PHS-3C (Shanghai Leici Scientific Instrument Co., Ltd., Shanghai, China, http://www.lei-ci.com). The CQDs were configurated by TG-16 High-speed centrifuge (Gongyi Yuhua Instrument Co., Ltd., Zhengzhou, China, http://www.gyyuhua.net/) and dried by LAB-1-50 freeze drier (Biocool Scientific Instrument Co., Ltd., Beijing, China, http://www.biocool.com.cn).

Preparation of MIP-CQDs and NIP-CQDs

The CQDs were synthesized by a facial one-step hydrothermal method according to the previous reports [33]. The syntheses were provided in the Electronic Supporting Material (ESM).

Briefly, 0.5 g chitosan powder was dissolved in 15 mL of 2% (v/v) acetic acid, and 5 mL of PFOS (400 mg·L^{-1}) was added and mixed for 3 h. Then 1.0 mg of CQDs and 200 μL of ECH were added, and then crosslinked with ECH at 40 °C for 8 h. After that, the solution was dropwise added into a vessel containing 500 mL NaOH (0.5 M). The chitosan beads were washed in acetone and NaOH (v/v = 1/1) for 8 h to remove the template, and finally rinsed with deionized water and freeze dried in a dryer until constant weight. The preparation of the non-imprinted polymer (NIP) adsorbent followed exactly the above procedure except the added template.

Detection of PFOS

To guarantee the template PFOS was eluted thoroughly from the MIP hydrogel, LC-MS detection method was developed for detection of PFOS. For MS operation, the ESI negative ion mode was applied, and the m/z 499 was selected for SIM mode. HPLC separation was performed using an Acquity UPLC™ BEN C_{18} column (100 mm × 2.1 mm, 1.7 μm). The mobile phase consisted 10 mM ammonium acetate/methanol (35/65, v/v), using flow rate of 0.2 mL min^{-1}. The linear equation between the concentration of 1–200 μg/L was developed.

For the fluorescent detection, a series of PFOS solutions were prepared in 2% HAc solution, and 1.0 g of MIP hydrogel beads were added. Then after shaking for 1 h, the solution was transferred to quartz cuvette and the PL intensity at 460 nm was measured at an excitation wavelength of 350 nm. (F- F_0)/F_0 was used as analytical signal where F_0 and F were the fluorescence intensity of the system in the absence and presence of the PFOS respectively.

The urine and serum samples were collected from healthy volunteers (kindly provided by South Medical University) and processed as follows. 5 mL of sample was placed into centrifuge tube. The tubes were centrifuged for 20 min at 12,000 rpm and 25 °C to remove protein, and the upper solution of 1 mL was withdrawn and diluted at 100-folds in aqueous solution. No further complex procedures were needed in the sample preparation. The fluorescence intensity at 460 nm was recorded at different concentration levels of PFOS.

Results and discussion

Characterization of the molecularly imprinted fluorescent chitosan hydrogel

The excitation-dependent photoluminescence (PL) behavior is observed in CQDs, as seen in the FL spectra in Fig. 1a. This behavior is contributed to the surface state affecting the band gap of CQDs [33]. The optimal excitation wavelength was 350 nm and emission wavelength was 460 nm. In comparison with CQDs, the excitation wavelength and emission wavelength of CQDs hydrogel red-shifted at about 15 nm and 7 nm respectively (Fig. 1b). It is probably due to hydrogel around the surface of CQDs changed the surface state and caused a red-shift of the CQDs emission [34].

The FT-IR spectra of MIP-CQDs and NIP-CQDs are shown in Fig. S1 (see supplementary material). The stretching vibration of C-OH (3430 cm^{-1}) and the vibrational absorption band of C=O at 1652 cm^{-1} were observed. The C-N vibration at 1080 cm^{-1} and 1380 cm^{-1} in chitosan decreased in MIP due to interaction between amino group in chitosan and sulfonate group in PFOS. The results showed that the binding sites were left in MIP after elution of PFOS. The morphology of MIP and NIP hydrogel were studied by SEM (Fig. 1c, d). Their surface morphologies were completely different. The NIP surface was smooth, while some pores in the nanometer level on the MIP surface were observed, which may form during the imprinting process and also be available after the removal of the templates.

In the UV/VIS spectra, the two peaks at 344 nm and 250 nm represented the absorbance of CQDs and chitosan (Fig. S2, see supplementary material). The morphology and structure of CQDs were studied by TEM. As shown in Fig. S3a (see supplementary material), the CQDs are about 5 nm. The XRD pattern of the CQDs also displayed a broad peak cantered at 20°, which is also attributed to highly disordered CQDs (Fig. S3b, see supplementary material). Furthermore, the QY of CQDs was 55% (using quinine sulphate as a reference).

Fluorometric determination of PFOS by using the MIP-CQDs

To confirm the enhancement of fluorescence intensity was caused by PFOS, the fluorescence intensity of MIP and NIP fluorescent hydrogel were compared (Fig. 2a, b). After removal of template PFOS, the fluorescence intensity of MIP hydrogel was decreased. However, no difference in the shape and position of the emission spectrum was observed on NIP-coated QDs. CQDs were doped on the chitosan hydrogel through covalent bond during the polymerization reaction of chitosan with epichlorohydrin (ECH). The nitrogen-doped CQDs are rich in amino groups. Upon addition of ECH, not only chitosan polymerizes with ECH, but also the CQDs are also copolymerized due to the reaction of amino groups in CQDs with ECH (ring-opening reaction). The results proved that the fluorescent intensity change was caused by PFOS, and also confirmed the elution process had little loss on PL intensity of MIP hydrogel.

When the PFOS was removed by solvent extraction with NaOH/acetone (1:1), imprinted binding sites were left in the hydrogel that were able to selectively rebind the target molecule PFOS. The -NH$_2$ groups on the surface of MIP-and NIP-coated CQDs acted as the binding sites to combine PFOS through hydrogen bond interactions or electrostatic interactions. Therefore, both the prepared MIP-and NIP-coated CQDs showed fluorescence response to the template PFOS. But many tailor-made recognition sites with complementarity to PFOS were produced, and the specific imprinted cavities in MIP hydrogel can generate a stronger adsorption of PFOS. The FL enhancement curves of MIP and NIP are shown in Fig.2c, d. The enhancement mechanism in the presence of PFOS was deduced as follows. The amino-groups have been reported to increase the surface passivation of CQDs. The pyridinic and pyrolic nitrogen atoms can be regarded as defect structures because they break the large conjugated carbon structure. The formation of these defects would lead to formation of more polyaromatic structures and give rise to stronger emission [35]. The sulfonate
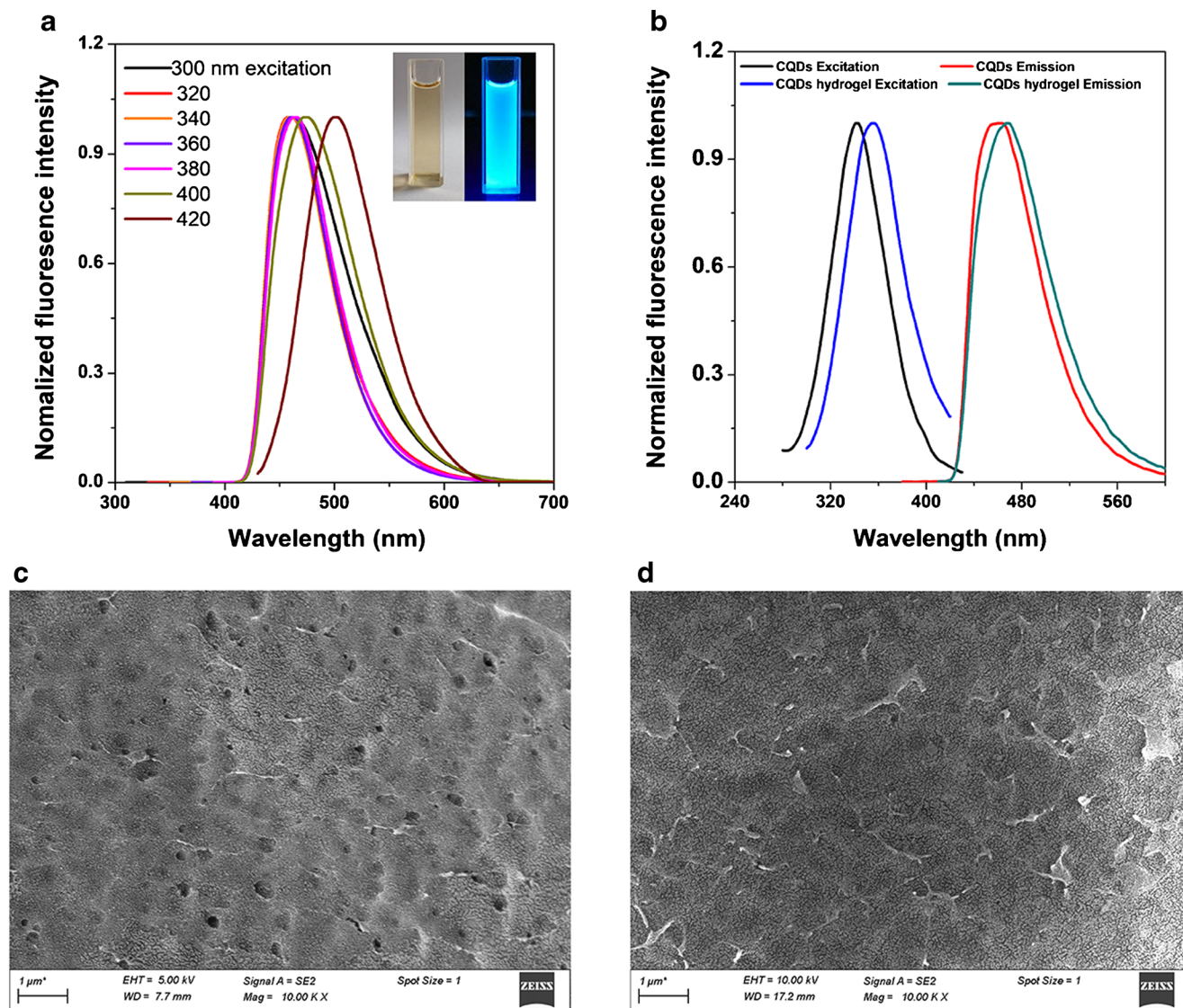
Fig. 1 Characteristic of MIP-CQDs hydrogel. **a** Excitation-dependent PL of CQDs. Inset: Photograph of the CQDs under illumination of white light (left) and UV (365 nm) light (right). **b** PL excitation and emission spectra of CQDs and MIP-CQDs hydrogel. **c** SEM result of MIP-CQDs hydrogel. **d** SEM result of NIP-CQDs hydrogel

group of PFOS can form complex with amino group through hydrogen bond or electrostatic reaction, which can enhance the conjugation degree of H_2N-passivated CQDs. As a result, the fluorescence emission was increased.

The FL enhancement in this system followed the equation. This equation was used to quantify the different constants in this research, and the ratio of the K_{SV} values of the MIP and NIP ($K_{SV, MIP}/K_{SV, NIP}$) was defined as the imprinting factor (IF) to evaluate the selectivity of the materials. The linear equations for MIP and NIP are illustrated in Fig. 3. Under optimum conditions the IF ($K_{sv, MIP}/K_{sv, NIP}$) is 2.75, which indicates that MIP-coated CQDs can recognize the template molecules. Compared with the NIP-coated ones, the MIP-coated CQDs have more binding sites suitable for the template PFOS due to an efficient imprinting effect.

Fluorometric determination in aqueous solution

Firstly, the influence of temperature and time for fluorescent detection were evaluated (Fig. S4, see supplementary material). The temperature has an important effect on the DNA conformation and its specific recognition on target. The temperature ranged from 20 °C to 40 °C was investigated. The results showed that high temperature was unfavorable for detection. Therefore, in this system, the reaction was performed at 25 °C, which provided a great convenience for practical application. The time was also examined. The results showed that the PL intensity reached equilibrium after 1 h.

The linear equation of the fluorescence intensity with the PFOS concentration ranged from 20 to 200 pg·L^{-1} are shown in Fig. 3. The PL intensity at 460 nm was recorded at
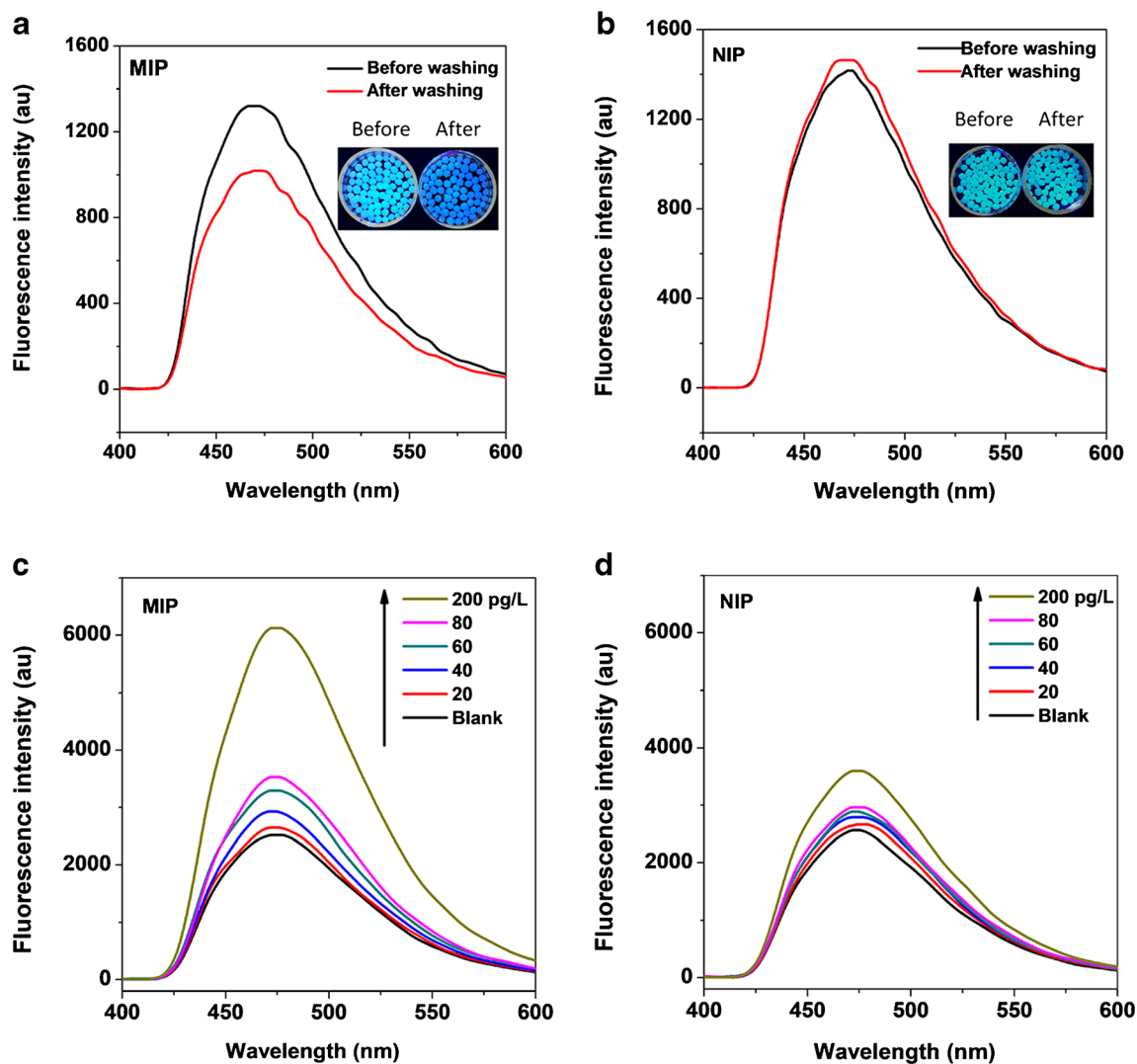
Fig. 2 **a** The PL spectra of MIP-CQDs hydrogel before and after elution of template. Inset: Photograph of the MIP-CQDs hydrogel before and after elution of template under UV (365 nm) light. **b** The PL spectra of NIP-CQDs hydrogel before and after elution of template. Inset: Photograph of the NIP-CQDs hydrogel before and after elution of template under UV (365 nm) light (**c**) The fluorescence recovery of MIP CQDs with various concentrations of PFOS (0, 20, 40, 60, 80 and 200 pg·L^{-1}). **d** The fluorescence recovery of NIP-CQDs with various concentrations of PFOS (0, 20, 40, 60, 80 and 200 pg·L^{-1})

excitation wavelength at 350 nm. With the increased concentration of PFOS, the PL intensity gradually increased. The LOD was calculated based on the $3\sigma/m$, (where σ is the standard deviation of the blank and m is the slope of the calibration plot) which was 0.4 pg·L^{-1}. The repeatability was obtained by 5 replicates analysis of spiked solution, the RSDs were less than 6.8%. Compared to the reported literature, the method was advantageous in high sensitivity and repeatability.

Specificity of the MIP-CQDs

In order to illustrate the selectivity of MIP-CQDs toward PFOS, control experiments were carried out to the analogues. The responses of MIP-CQDs and NIP-CQDs to different concentrations of analogues, and the linear relationships with MIP and NIP are shown in Fig. S5-S11 (see supplementary material). All the K_{sv} values of MIP-CQDs and NIP-CQDs to analogs and PFOS are compared in Fig. 4. As expected, the K_{sv} for PFOS was much higher than those of its structural analogs, and also IF 2.75 was highest, which indicated an efficient imprinting effect. The IF value for analogues were ranged from 0.51 to 1.33, indicating that there were no selective recognition sites. Molecular that has sulfonate group such as PFBS, SDS', OSA and PFSF had smaller fluorescence ratios than PFOS. The shorter chain length of PFBS, as well as smaller steric hindrance of SDS' and OSA, the less enhancement consequent of CQDs was observed. For molecular SDS and SDBS which had no sulfate group, the PL intensity was quenched instead of enhancement. The

Fig. 3 The linear relationship between the fluorescence recovery and the concentration of PFOS within the range of 20–200 pg·L^{-1}. **a** MIP. **b** NIP

a MIP

$y = 0.0055x - 0.017$

b NIP

$y = 0.002x + 0.00030$
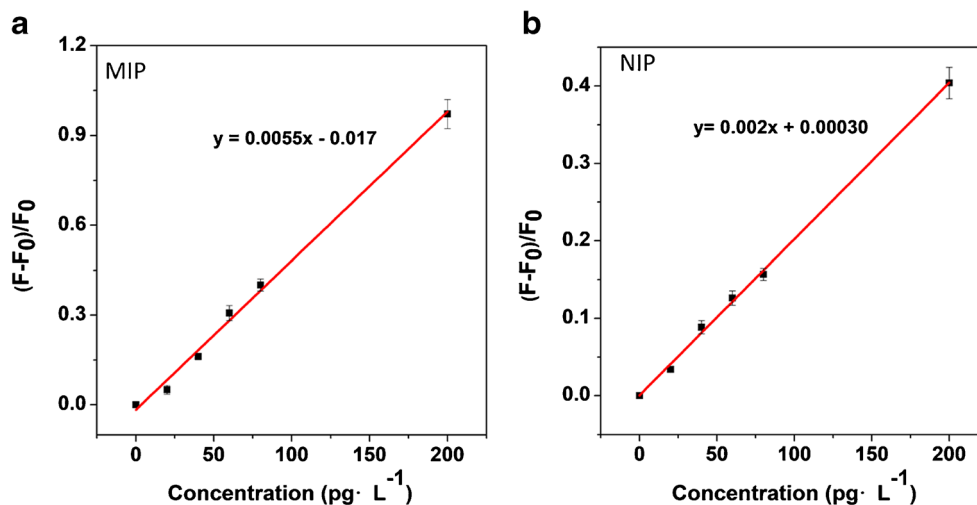
PFOA also had enhancement effect on PL intensity of CQDs with much lower K_{sv} compared to PFOS. The imprinted binding sites (cavities) play an important role in the selective luminescence response to PFOS. It is known that the well-defined structure of the imprinted cavities can be exploited for the rebinding of template molecules. However, the imprinted cavity of MIP-QDs is not suitable to accommodate the other compounds, which results in the selective FL response to PFOS. In order to apply the MIP-CQDs in the complex samples, the co-existing substances such as common ions, sugars and human serum albumin, etc. in the matrix were evaluated (Fig. 4b). It showss that little interference is found on the MIP-CQDs, which once again proves the robustness of the method.

## Fluorometric determination of PFOS in serum and urine

The serum samples were firstly diluted at about 100 folds, and spiked with PFOS with concentrations ranged from 20 to 200 pg·L^{-1}. With the increased concentration of PFOS, the PL intensity of CQDs increased gradually as in aqueous solution. The PL intensity at 460 nm was recorded at excitation wavelength at 350 nm. The background signal was higher in aqueous solution, since serum samples were complex biological samples which contains a lot of biomolecules and proteins, etc. The linear equation was developed and it was similar as before (Fig. 5). The slightly higher LOD in the serum matrix was 66 pg·L^{-1}. For the urine samples, the equation was similar to the serum, and detection limit was 85 pg·L^{-1}. These results have shown high robustness of the MIP-CQDs for detection of PFOS in the complex matrix.

Method validation

Three different urine samples and serum samples were pretreated and tested as follows. The serum samples and urine samples were firstly diluted and introduced to the MIP-CQDs. The results are shown in Table 1. The PFOS level in serum and urine samples were below the LODs. Furthermore, standard addition experiments were performed with these serum

Fig. 4 **a** The K_{sv} of MIP-CQDs towards different analogues. K_{sv} represented the slope of relationship between a series of concentrations of analogue and PL intensity of MIP or NIP-CQDs. **b** Relative fluorescence intensity (F/F_0) of the MIP-CQDs in the presence and absence of different interferences. The concentrations of all compounds were 0.05 M
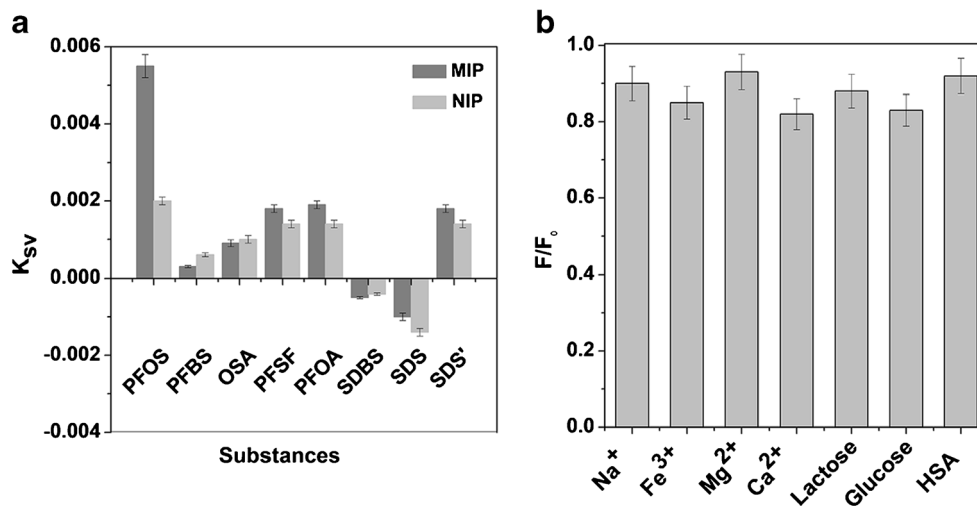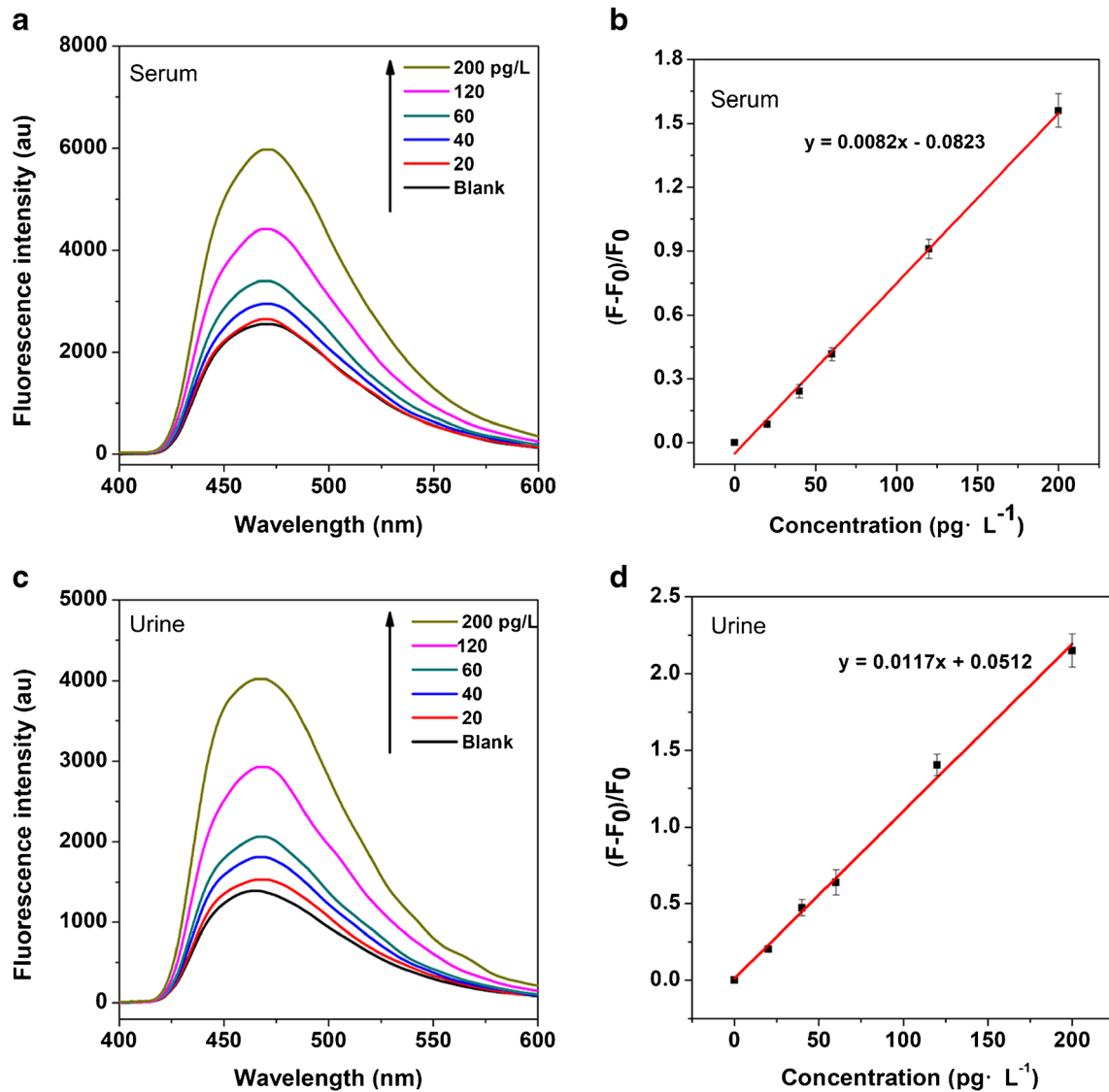
Fig. 5 a The fluorescence recovery of MIP hydrogel with various concentrations of PFOS in serum samples (0, 20, 40, 80, 120 and 200 pg·L^{-1}). b The fluorescence intensity changes with the concentration of PFOS in the range of 20–200 pg·L^{-1}. c The fluorescence recovery of MIP hydrogel with various concentrations of PFOS in urine samples (0, 20, 40, 80, 120 and 200 pg·L^{-1}). d The linear relationship between the fluorescence recovery and the concentration of PFOS within the range of 20–200 pg·L^{-1}

Table 1   Analytical results of the direct determination of PFOS in serum and urine samples using fluorescent MIP hydrogel

Serum	Measured	Added (pg/L)	Found (pg/L)	Recovery (%)	RSD ($n = 3$, %)
1	na	25.0	21.7	87	1.8
2	na	50.0	47.5	95	6.7
3a	na	2.0 μg L^{-1}	1.96 μg L^{-1}	98	3.5
3b	na	200	178	89	5.6
Urine	Measured	Added (pg/L)	Found (pg/L)	Recovery (%)	RSD ($n = 3$, %)
1	na	25.0	20.2	81	5.5
2	na	50.0	45.0	90	7.9
3a*	na	2.0 μg L^{-1}	1.83 μg L^{-1}	92	4.3
3b*	na	200	190	95	8.2

*3a sample were first determined by LC-MS/MS, and diluted 10 thousand times to obtain 3b samples. 3b sample was determined by MIP fluorescence method

Table 2   Comparison with other methods for PFOS detection

Method	Sample	LODs	reference
LC-MS	environmental water samples	3.2 pgmL^{-1},	[5]
LC-MS/MS	Food packaging	<0.05 μg L^{-1},	[6]
Fluorescent	Tap water and river water	5.57 μg L^{-1}.	[7]
Photoelectrochemical	water samples	86 ng mL^{-1}	[8]
MIP-fluorescent	Serum and urine	0.66 and 0.85 pg/L	This work

samples to validate the determination. The recoveries were from 81 to 98%. The repeatability was obtained by 3 replicates analysis of spiked solution, with RSDs ranged from 1.8–82% (Table 1), which are acceptable for quantitative assays performed in real complex samples. The results were validated by its comparison with totally independent technique of LC-MS/MS method. The linear equation with the PFOS concentration range of 1–200 μg/L was developed. The equation was $Y = -3384.7 + 213.3X$ with correlation coefficient 0.995. The result of spike-recovery test by LC-MS/MS was shown in Table 1, which were consistent with the developed fluorescence method of MIP based on CQDs.

The analytical methods for PFOS detection have been reported and some of them were summarized and compared with our work in Table 2. Detection of PFOS by LC-MS/MS is commonly applied method with high accuracy and stability, but needs long manipulation time, extensive sample preparation and highly skilled personnel [5, 6]. Compared with LC-MS/MS method, fluorescence analysis method has a lot of advantages, such as test rapidity and also high sensitivity. The fluorescence method using dye-(NH_2)-SiO$_2$NPs and TiO$_2$ nanotube arrays were also reported. In contrast, portable molecular imprinting chitosan hydrogel proposed in our study is eco-friendly material and sensitive enough for PFOS detection. Furthermore, the material that we used in this method has high selectivity because of using MIP technique.

Conclusion

A molecularly imprinted chitosan hydrogel bead doped with CQDs was applied for detection of PFOS in complex samples. The hydrogel bead is convenient for elution of template and separation from matrix samples. The imprinting factor of 2.75 indicated high selectivity of the method toward PFOS. Besides, the "turn on" detection mode make the LOD lower than other quench assays. The method can be potential indicator for monitoring the PFOS removal in environmental samples, for the fluorescence emission of the MIP hydrogel can be visualized under UV lamp by naked eye. The limitation of the method is that MIP hydrogel is irreversible, as the the shape of

hydrogel bead is apt to be destroyed during elution of PFOS by NaOH. In the future, the reversible MIP hydrogel is expected to be developed to reduce the cost for application.

Compliance with ethical standards The author(s) declare that they have no competing interests.

References

1. Houde M, Czub G, Small JM, Backus S, Wang X, Alaee M, Muir DC (2008) Fractionation and bioaccumulation of perfluorooctane sulfonate (PFOS) isomers in a Lake Ontario food web. Environ Sci Technol 42:9397–9403. https://doi.org/10.1021/es800906r

2. Loos R, Wollgast J, Huber T, Hanke J (2007) Polar herbicides, pharmaceutical products, perfluorooctanesulfonate (PFOS), perfluorooctanoate (PFOA), and nonylphenol and its carboxylates and ethoxylates in surface and tap waters around Lake Maggiore in northern Italy. Anal Bioanal Chem 387:1469–1478. https://doi.org/10.1007/s00216-006-1036-7

3. Tittlemier SA, Pepper K, Seymour C, Moisey J, Bronson R, Cao XL, Dabeka RD (2007) Dietary exposure of Canadians to perfluorinated carboxylates and perfluorooctane sulfonate via consumption of meat, fish, fast foods, and food items prepared in their packaging. J Agric Food Chem 55:3203–3210. https://doi.org/10.1021/es800906r

4. Olsen GW, Mair DC, Reagen WK, Ellefson ME, Ehresman DJ, Butenhoff JL, Zobel LR (2007) Preliminary evidence of a decline in perfluorooctanesulfonate (PFOS) and perfluorooctanoate (PFOA) concentrations in American red Cross blood donors. Chemosphere 68:105–111. https://doi.org/10.1016/j.chemosphere.2006.12.031

5. Saito K, Uemura E, Atsushi I, Hiroyuki K (2010) Determination of perfluorooctanoic acid and perfluorooctane sulfonate by automated in-tube solid-phase microextraction coupled with liquid chromatography-mass spectrometry. Anal Chim Acta 658:141–146. https://doi.org/10.1016/j.aca.2009.11.004

6. Poothong S, Boontanona SK, Boontanonb N (2012) Determination of perfluorooctane sulfonate and perfluorooctanoic acid in food packaging using liquid chromatography coupled with tandem mass spectrometry. J Hazard Mater 205:139–143. https://doi.org/10.1016/j.jhazmat.2011.12.050

7. Feng H, Wang NY, ThanhThuy TT, Yuan LJ, Li JZ, Cai QY (2014) Surface molecular imprinting on dye-(NH_2)-SiO$_2$ NPs for specific recognition and direct fluorescent quantification of perfluorooctane sulfonate. Sensors Actuators B Chem 195:266–273. https://doi.org/10.1016/j.snb.2014.01.036

8. ThanhThuy TT, Li JZ, Feng H, Cai J, Yuan LJ, Wang NY, Cai QY (2014) Molecularly imprinted polymer modified TiO$_2$ nanotube arrays for photoelectrochemical determination of perfluorooctane sulfonate (PFOS). Sensors Actuators B Chem 190:745–751. https://doi.org/10.1016/j.snb.2013.09.048

9. Yang S, Li Y, Wang S, Wang M, Chu M, Xia B (2018) Advances in the use of carbonaceous materials for the electrochemical determination of persistent organic pollutants. A review. Microchim Acta 185(112). https://doi.org/10.1007/s00604-017-2638-9

10. Chen SH, Li AM, Zhang LZ, Gong JM (2015) Molecularly imprinted ultrathin graphitic carbon nitride nanosheets based electrochemiluminescence sensing probe for sensitive detection of perfluorooctanoic acid. Anal Chim Acta 896:68–77. https://doi.org/10.1016/j.aca.2015.09.022

11. Hua XG, Pana JL, Hua YL, Li GK (2009) Preparation and evaluation of propranolol molecularly imprinted solid-phase microextraction fiber for trace analysis of β-blockers in urine and plasma samples. J Chromatogr A 1216:190–197. https://doi.org/10.1016/j.chroma.2008.11.064

12. Xu ZG, Hu YF, Hu YL, Li GK (2010) Investigation of ractopamine molecularly imprinted stir bar sorptive extraction and its application for trace analysis of β-agonists in complex samples. J Chromatogr A 1217:3612–3618. https://doi.org/10.1016/j.chroma.2010.03.046

13. Liu HL, Fang GZ, Wang S (2014) Molecularly imprinted optosensing material based on hydrophobic CdSe quantum dots via a reverse microemulsion for specific recognition of ractopamine. Biosens Bioelectron 55:127–132. https://doi.org/10.1016/j.bios.2013.11.064

14. Ren XH, Liu HC, Chen LG (2015) Fluorescent detection of chlorpyrifos using Mn (II)-doped ZnS quantum dots coated with a molecularly imprinted polymer. Microchim Acta 182:193–200. https://doi.org/10.1007/s00604-014-1317-3

15. Dan L, Wang HF (2013) Mn-doped ZnS quantum dot imbedded two-fragment imprinting silica for enhanced room temperature phosphorescence probing of domoic acid. Anal Chem 85:4844–4848. https://doi.org/10.1021/ac400250j

16. Ren XH, Chen LG (2015) Quantum dots coated with molecularly imprinted polymer as fluorescence probe for detection of cyphenothrin. Biosens Bioelectron 64:182–188. https://doi.org/10.1016/j.bios.2014.08.086

17. Liu JX, Chen H, Lin Z, Lin JM (2010) Preparation of surface imprinting polymer capped Mn-doped ZnS quantum dots and their application for chemiluminescence detection of 4-nitrophenol in tap water. Anal Chem 82:7380–7386. https://doi.org/10.1021/ac101510b

18. Chen YP, Wang DN, Yin YM, Wang LY, Wang XF, Xie MX (2012) Quantum dots capped with dummy molecularly imprinted film as luminescent sensor for the determination of tetrabromobisphenol a in water and soils. J Agric Food Chem 60:10472–10479. https://doi.org/10.1021/jf3026138

19. Wang HF, He Y, Ji TR, Yan XP (2009) Surface molecular imprinting on Mn-doped ZnS quantum dots for room-temperature phosphorescence optosensing of pentachlorophenol in water. Anal Chem 81:1615–1621. https://doi.org/10.1021/ac802375a

20. Li HB, Li YL, Cheng J (2010) Molecularly imprinted silica nanospheres embedded CdSe quantum dots for highly selective and sensitive optosensing of pyrethroids. Chem Mater 22:2451–2457. https://doi.org/10.1021/cm902856y

21. Xu SF, Lu HZ, Li JH, Song XL, Wang AX, Chen LX, Han SB (2013) Dummy molecularly imprinted polymers-capped CdTe quantum dots for the fluorescent sensing of 2,4,6-trinitrotoluene. ACS Appl Mater Interfaces 5:8146–8154. https://doi.org/10.1021/am4022076

22. Zhou Y, Qu ZB, Zeng YB, Zhou TS, Shi GY (2014) A novel composite of graphene quantum dots and molecularly imprinted polymer for fluorescent detection of paranitrophenol. Biosens Bioelectron 52:317–323. https://doi.org/10.1016/j.bios.2013.09.022

23. Liu HL, Fang GZ, Zhu HD, Li CM, Liu CC, Wang S (2013) A novel ionic liquid stabilized molecularly imprinted optosensing material based on quantum dots and graphene oxide for specific recognition of vitamin E. Biosens Bioelectron 47:127–132. https://doi.org/10.1016/j.bios.2013.03.006

24. Hao TF, Wei X, Nie YJ, Xu YQ, Yan YS, Zhou ZP (2016) An eco-friendly molecularly imprinted fluorescence composite material based on carbon dots for fluorescent detection of 4-nitrophenol. Microchim Acta 183:2197–2203. https://doi.org/10.1007/s00604-016-1851-2

25. Chen BB, Liu ZX, Deng WC, Zhan L, Liu ML, Huang CZ (2016) A large-scale synthesis of photoluminescent carbon quantum dots: a self-exothermic reaction driving the formation of the nanocrystalline core at room temperature. Green Chem 18:5127–5132. http://pubs.rsc.org/en/content/articlehtml/2016/gc/c6gc01820c

26. Wu ZL, Zhang P, Gao MX, Liu CF, Wang W, Leng F, Huang CZ (2013) One-pot hydrothermal synthesis of highly luminescent nitrogen-doped amphoteric carbon dots for bioimaging from Bombyx mori silk-natural proteins. J Mater Chem B 122:2868–2873. https://doi.org/10.1039/C6GC01820C

27. Zhou J, Yang Y, Zhang CY (2013) A low-temperature solid-phase method to synthesize highly fluorescent carbon nitride dots with tunable emission. Chem Commun 49:8605–8607. https://doi.org/10.1039/C3CC42266F

28. Zhao HX, Liu LQ, De Liu Z, Wang Y, Zhao XJ, Huang CZ (2011) Highly selective detection of phosphate in very complicated matrixes with an off-on fluorescent probe of europium-adjusted carbon dots. Chem Commun 47:2604–2606. https://doi.org/10.1039/C0CC04399K

29. Yang Q, Wei L, Zheng X, Xiao L (2015) Single particle dynamic imaging and Fe^{3+} sensing with bright carbon dots derived from bovine serum albumin proteins. Sci Rep 5(17727). https://doi.org/10.1038/srep17727

30. Ma Y, Zhang Z, Xu Y, Ma M, Chen B, Wei L, Xiao L (2016) A bright carbon-dot-based fluorescent probe for selective and sensitive detection of mercury ions. Talanta 161:476–481. https://doi.org/10.1016/j.talanta.2016.08.082

31. Yu Q, Deng SB, Yu G (2008) Selective removal of perfluorooctane sulfonate from aqueous solution using chitosan-based molecularly imprinted polymer adsorbents. Water Res 42:3089–3097. https://doi.org/10.1016/j.watres.2008.02.024

32. Hu L, Li Y, Zhang WL (2016) Characterization and application of surface-molecular-imprinted-polymer modified TiO_2 nanotubes for removal of perfluorinated chemicals. Water Sci Technol 74:1417–1425. https://doi.org/10.2166/wst.2016.321

33. Qian Z, Ma J, Shan X, Feng H, Shao L, Chen J (2014) Highly luminescent N-doped carbon quantum dots as an effective multifunctional fluorescence sensing platform. Chem Eur J 20:2254–2263. https://doi.org/10.1002/chem.201304374

34. Chandra S, Pathan SH, Mitra S, Modha BH, Goswami A, Pramanik P (2012) Tuning of photoluminescence on different surface functionalized carbon quantum dots. RSC Adv 2:3602–3606. http://pubs.rsc.org/en/content/articlehtml/2012/ra/c2ra00030j

35. Zuo P, Lu X, Sun Z, Guo Y, He H (2016) A review on syntheses, properties, characterization and bioanalytical applications of fluorescent carbon dots. Microchim Acta 183:519–542. https://doi.org/10.1007/s00604-015-1705-3